New superconducting and semiconducting Fe-B compounds predicted with an *ab initio* evolutionary search

A.N. Kolmogorov,[1] S. Shah,[1] E.R. Margine,[1] A.F. Bialon,[2] T. Hammerschmidt,[2] and R. Drautz[2]
[1] *Department of Materials, University of Oxford, Parks Road, Oxford OX1 3PH, United Kingdom and*
[2] *Atomistic Modelling and Simulation, ICAMS, Ruhr-Universität Bochum, D-44801 Bochum, Germany*
(Dated: February 17, 2022)

New candidate ground states at 1:4, 1:2, and 1:1 compositions are identified in the well known Fe-B system via a combination of *ab initio* high-throughput and evolutionary searches. We show that the proposed oP12-FeB_2 stabilizes by a break up of 2D boron layers into 1D chains while oP10-FeB_4 stabilizes by a distortion of a 3D boron network. The uniqueness of these configurations gives rise to a set of remarkable properties: oP12-FeB_2 is expected to be the first semiconducting metal diboride and oP10-FeB_4 is shown to have the potential for phonon-mediated superconductivity with a T_c of 15-20 K.

PACS numbers: 61.66.Fn, 74.10.+v, 71.20.Ps

A range of advanced compound prediction methods has been developed recently to accelerate the experimental search for materials displaying novel physics or technologically relevant features [1–4]. Unconstrained structural optimization with evolutionary algorithms (EAs) has shown the ability to predict complex configurations given only the composition leading to identification of exotic high-pressure phases [3]. High-throughput screening with data mining techniques has proven effective in revealing compositions favorable to form in large sets of multi-component systems [4]. In this study we demonstrate that new ambient-pressure materials with appealing properties could be found in such a well-known and accessible binary system as Fe-B.

The experimental research on Fe-B compounds has been driven primarily by their potential to serve as a hardening agent in steels [5] or as hard protective coatings [6, 7]. According to the latest experimental phase diagram [8], FeB and Fe_2B are the only reproducible low temperature phases that have been shown to crystallize in the oP8 (or the related oS8 [9]) and tI12 configurations, respectively. Less is known about the boron-rich ordered phases with only a few reports available: observation of a metastable FeB_{49} intercalation compound [10] and possible synthesis of amorphous [11] and the AlB_2-type [12] iron diborides. Previous modelling work on Fe-B compounds has given insights into their binding, magnetic, and structural properties [13–18] but has not systematically explored the possibility of obtaining new stable iron borides.

Our reexamination of the Fe-B system within density functional theory (DFT) begins with a high-throughput scan of known configurations listed in the Inorganic Crystal Structure Database ICSD [19]. We show that never observed oP6-FeB_2 (hP6-FeB_2) and tI16-FeB phases are marginally stable relative to the known compounds. The proposed Fe-B ground states are then refined with an *ab initio* evolutionary search that suggests oP10-FeB_4 and oP12-FeB_2 to be ground states at 1:4 and 1:2 compositions. The prediction of the brand new stable structure types is surprising as transition metal (TM) borides tend to crystallize in configurations correlating well between the 3*d*, 4*d*, and 5*d* series [20]. We link the stabilization of the Fe-B phases to the structural changes in the B networks that lead to radically new properties. At 1:2 metal-boron composition, famous for the outstanding MgB_2 superconductor [21] and the hardest metal-based ReB_2 material [22], oP12-FeB_2 stands out as the first semiconducting metal diboride made out of B chains rather than B layers. At 1:4 composition, the nonmagnetic oP10-FeB_4 is examined using electron-phonon (*e*-ph) calculations and predicted to be, subject to spin fluctuation effects [23], a superconductor with an unexpectedly high T_c of 15-20 K. The critical temperature falls between the typical 10 K T_c of TM borides [24] and the 39 K T_c of MgB_2 [21]. If synthesized, oP10-FeB_4 could extend the family of recently discovered iron-based $LaFeAsO_{1-x}F_x$ and FeSe superconducting materials [25] but have the conventional phonon-mediated coupling mechanism.

We carry out the high-throughput scan by calculating formation enthalpies at $T = 0$ K and $P = 0$ GPa with VASP [26] for over 40 commonly observed M-B and M-C ICSD structure types [27] in the whole composition range. The B-rich end of the phase diagram is further explored with the Module for *Ab Initio* Structure Evolution (MAISE) [28] linked with VASP which enables an EA search for the lowest enthalpy ordered phases. The unconstrained structural optimization is carried out for most likely to occur 1:6, 1:4, 1:3, and 1:2 compositions starting from random unit cells of up to 15 atoms (for further details see supplementary material [27]).

Finding ground states also depends on the accuracy of the simulation method and the inclusion of important Gibbs energy contributions [1]. We use the projector augmented waves method [29] and allow spin polarization unless stated otherwise; the chosen energy cutoff of 500 eV and dense Monkhorst-Pack k-meshes [30] ensure numerical convergence of formation energy differences

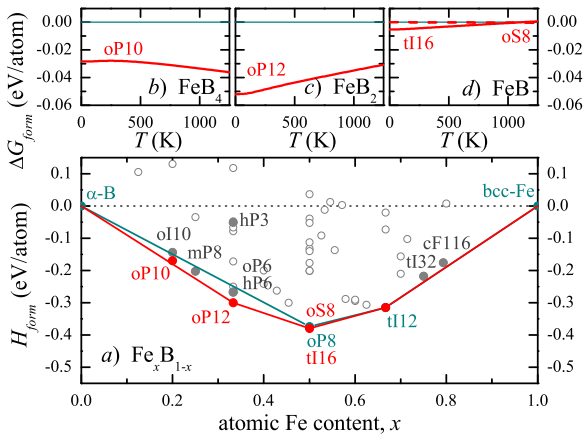

FIG. 1: (Color online) Stability of Fe-B alloys calculated with GGA-PBE: *a*) formation enthalpy; *b*-*d*) Gibbs energy with thermodynamic corrections due to the vibrational entropy for selected candidate phases w.r.t. the α-B↔oP8-FeB tie-line.

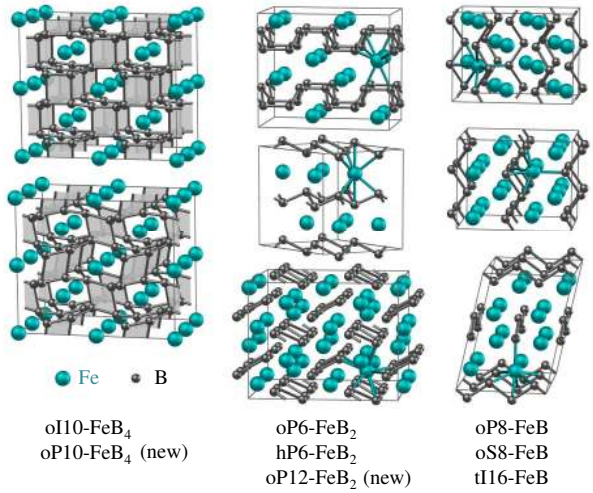

FIG. 2: (Color online) Competing B-rich Fe-B phases; cell parameters are given in the supplementary material [27].

to typically 1-2 meV/atom. We employ the Perdew-Burke-Ernzerhof (PBE) exchange-correlation (xc) functional [31] within the generalized gradient approximation (GGA) that provides a realistic description of the Fe ground state [32]. Tests in the supplementary material [27] demonstrate independence of our key finding, the stability of new phases at the 1:2 and 1:4 Fe-B compositions with respect to known compounds, on the choice of the xc functional. The ground state of B is modelled as α-B which has been recently shown to be only 3-4 meV/atom above the more complex β-B in the 0-300 K temperature range [33]. We include phonon corrections to $G(T)$ using a finite displacement method as implemented in PHON [34]. The *e*-ph calculations are carried out within the linear response theory using the Quantum-ESPRESSO package [35, 36]. Our tests show no magnetic moment in relevant B-rich phases allowing us to do the EA, phonon, and *e*-ph simulations without spin polarization.

Figure 1(a) summarizes calculated $T = 0$ K formation energies of the considered Fe_xB_{1-x} ordered structures with the convex hull drawn (in cyan) through the known oP8-FeB and tI12-Fe_2B ground states; other relevant oI10, oP10, mP8, hP3, hP6, oP6, oP12, oS8, tI16, tI32 and cF116 structures correspond to the CrB_4, FeB_4 (proposed), FeB_3 (proposed), AlB_2, ReB_2, RuB_2, FeB_2 (proposed), CrB, MoB, Ni_3P, and $Cr_{23}C_6$ prototypes, respectively. Phases with $x > 0.5$ show an expected ordering, with tI12-Fe_2B being stable and Fe_3B and $Fe_{23}B_6$ being metastable by less than 20 meV/atom. For $x \leq 0.5$, we find a set of phases that are below or close to the α-B↔oP8-FeB tie-line to be viable ground state candidates. We discuss their relative stability using structural and electronic density of states (DOS) information shown in Figs. 2 and 3.

The similarity of the local coordinations in oP8, oS8, and tI16 at 1:1 composition was discussed previously in Ref. [37]. In tI16 the B chains extend in two directions, a feature that could differentiate the structure's mechanical response to external load from the behaviour of the other two polymorphs. Fig. 1(d) reflects the difference in the vibrational properties of oP8 (oS8) and tI16 and could explain why tI16-FeB, marginally the most stable phase at $T = 0$ K in our calculations, has never been observed. The electronic DOS of FeB in the three configurations are rather similar (Fig. 3): they are all metallic and magnetic and have bonding *p*-*d* hybridized states in the -6 - -3 eV energy range.

At 1:2 composition, all known metal borides stable under normal conditions are composed of 2D boron layers that are flat in hP3, armchair in oP6, zigzag in hP6, or mixed in hR18 [19]. A detailed rigid band approximation study of the TMB_2 phases linked the distortion of the B layers to population of antibonding TM-TM and TM-B orbitals in hP3-TMB_2 with high *d*-electron count [13]. The projected DOS in hP3-FeB_2 (Fig. 3) shows a mismatch in the maxima of the filled B and Fe states in the -7 - -3 eV range and a high DOS at the Fermi level resulting in a magnetic moment of 0.26 μ_B/atom. The magnetisation energy of 11 meV/atom is insufficient to stabilize the hP3-FeB phase which leaves it 200 meV/atom above the α-B↔oP8-FeB tie-line. Puckering of the B layers in non-magnetic oP6 and hP6 proves to be a more favorable way of reducing the high DOS at the Fermi level: Fig. 3 shows a higher hybridization of the B-*p* and Fe-*d* states with the antibonding $p-d$ states now lying just above E_F. The net result of the more bimodal shape of the DOS is a 217 meV/atom gain in stability. Even more dramatic structural and electronic changes take place in oP12-FeB_2 discovered in our EA search. The disintegration of the B layers opens up a ~ 0.5 eV band gap (likely underestimated in our semilo-

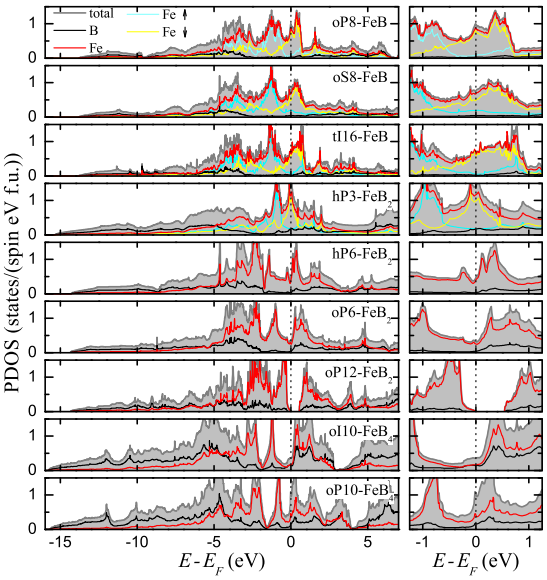

FIG. 3: (Color online) Calculated density of states in selected iron borides (the lower five compounds are non-magnetic).

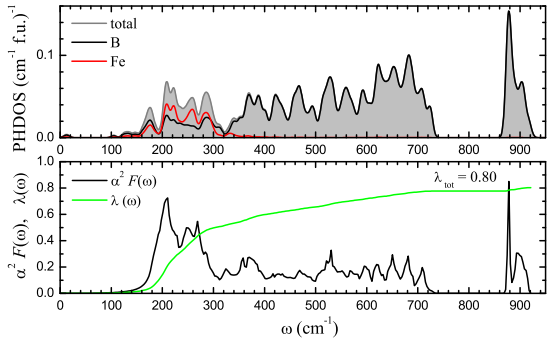

FIG. 4: (Color online) Top: total and projected phonon density of states (PHDOS) in oP10-FeB_4. Bottom: Eliashberg function and the strength of the electron-phonon coupling.

cal DFT treatment [38]) and leads to an additional 33 meV/atom gain in stability. This finding rules out the existence of hP3-FeB_2 that has been a subject of controversy [39]; oP12-FeB_2 is below the α-B↔oP8-FeB tie-line by over 30 meV/atom (Fig. 1(c)) in the whole T range and should be synthesizable.

At 1:3 composition, the EA suggests a new mP8 phase [27] that breaks the α-B↔oP8-FeB tie-line by 15 meV/atom; however it is found to be metastable w.r.t. α-B and oP12-FeB_2 at all temperatures.

At 1:4 composition, the observed proximity of the oI10-FeB_4 phase to the α-B↔oP8-FeB tie-line is intriguing as there have been explicit references to unsuccessful attempts to synthesize this phase [14]. Unexpectedly, a phonon dispersion calculation showed dynamical instability of oI10-FeB_4, with imaginary frequencies reaching $208i$ cm^{-1} for a Γ-point phonon in the conventional 10-atom unit cell. Using the phonon eigenvector that skews the rectangle B building units in the x-y plane into parallelograms we have constructed a new structure type, oP10-FeB_4. The considerable energy gain of 28 meV/atom and no imaginary frequencies in the phonon spectrum make oP10-FeB_4 thermodynamically and dynamically stable in the considered temperature range relative to known phases [Fig. 1(b)]; with phonon corrections included oP10-FeB_4 lies 3 meV/atom above the α-B↔oP12-FeB_2 tie-line at $T = 0$ K but 10 meV/atom below the tie-line at $T = 900$ K. Additional no-symmetry relaxations of distorted oI10 and oP10 supercells with 10, 20, and 40 atoms have consistently produced oP10-FeB_4 as the most stable configuration. The EA search has also shown that Fe_2B_8 cells converge to oP10-FeB_4 while Fe_3B_{12} cells evolve into a new mS30-FeB_4 phase metastable by 6 meV/atom. The tests seemed necessary due to a counterintuitive evolution of the DOS in the oI10 to oP10 transformation: the Fermi level in oP10-FeB_4 catches the edge of the antibonding $p_{x,y}$-$d_{x^2-y^2}$ peak resulting in a high $n(E_F) = 1.0$ states/(eV spin f.u.); the feature is unusual as stable compounds tend to have the Fermi level lying in the pseudogap [40].

The naturally electron-doped oP10-FeB_4 candidate material with strong covalent bonds is next analyzed for superconducting features. We use the linear response theory and fine k- and q-meshes [27, 36] to calculate the phonon DOS (PHDOS), Eliashberg function ($\alpha^2F(\omega)$), and strength of the e-ph coupling ($\lambda(\omega)$). The phonon spectrum in Fig. 4 can be divided into three regions with mixed Fe-B modes (0-320 cm^{-1}), B modes with a relatively flat PHDOS (320-740 cm^{-1}), and B modes involving in-plane optical distortions of B parallelograms (860-920 cm^{-1}). The Eliashberg function integrates to a large $\lambda_{\rm tot} = 0.80$ and gives the logarithmic average $\langle\omega\rangle_{ln} = 430$ cm^{-1}. While key contributions to $\lambda_{\rm tot} \sim 0.8$ in CaC_6 and MgB_2 come from the low-frequency Ca modes ($\omega < 150$ cm^{-1}) [41] and the high-frequency B modes (500 cm^{-1} $< \omega <$ 560 cm^{-1}) [42], respectively, nearly 60% of $\lambda_{\rm tot}$ in oP10-FeB_4 is generated by the mixed Fe-B modes in the 160-300 cm^{-1} range. $\langle\omega\rangle_{ln}$ in oP10-FeB_4 is found to be much closer to the MgB_2 value of $\sim$ 450 cm^{-1} [42], rather than the CaC_6 value of $\sim$ 200 cm^{-1} [41]. Using the Allen-Dynes formula [43] and typical μ^* of 0.14-0.10 we estimate the T_c in oP10-FeB_4 to be 15-20 K. The compound has two 3D Fermi surfaces centered at Γ and R points and the T_c may be further enhanced by the multiband effect. Because of the large gradient of the DOS near the Fermi level the superconducting properties may be strongly affected by the presence of vacancies or impurities. Although oP10-FeB_4 is found to have neither ferro- nor antiferromagnetic moment, spin fluctuations [23] could play a critical role in the pairing mechanism and should be examined carefully using input from experiment.

In summary, our search for new compounds in the common Fe-B system demonstrates the necessity to go beyond standard structure types: The EA-driven unconstrained structural optimization has uncovered a set of viable ground states, with new oP10-FeB_4 and oP12-FeB_2 shown to be thermodynamically stable by over 25 meV/atom relative to the known α-B and oP8-FeB. To the best of our knowledge, the identified boron-rich phases have been never observed before and their discovery may require finding suitable kinetic routes. The presented analysis of the structural and electronic properties shows how the phases stabilize and what new physics they are expected to exhibit if synthesized. (i) oP10-FeB_4 could become yet another exception to Matthias' rules [44] that recommend staying away from magnetic elements when designing new superconductors. This compound has a high DOS at the Fermi level leading to $\lambda = 0.80$ and a surprisingly high T_c of 15-20 K. (ii) oP12-FeB_2 is predicted to be the first metal diboride semiconductor with a ~ 0.5 eV band gap (time-dependent DFT or Green's functions techniques will likely give a larger value [38]). (iii) The proposed materials may also exhibit appealing mechanical properties as hardness tends to be higher for M_xB_{1-x} with $x < 0.5$ [22].

ANK and SS acknowledge the support of the EPSRC and the Oxford Supercomputing Centre. AFB, TH and RD acknowledge financial support through ThyssenKrupp AG, Bayer MaterialScience AG, Salzgitter Mannesmann Forschung GmbH, Robert Bosch GmbH, Benteler Stahl/Rohr GmbH, Bayer Technology Services GmbH and the state of North-Rhine Westphalia as well as the EU in the framework of the ERDF.

[1] S.W. Woodley and R. Catlow, Nature Mater., **7**, 937 (2008).
[2] R. Martoňák, A. Laio, and M. Parrinello, Phys. Rev. Lett. **90**, 075503 (2003); S. Curtarolo *et al.*, Phys. Rev. Lett. **91**, 135503 (2003); C.C. Fischer *et al.*, Nat. Mater. **5**, 641 (2006); G. Trimarchi, A.J. Freeman, and A. Zunger, Phys. Rev. B **80**, 092101 (2009); C.J. Pickard and R.J. Needs, Phys. Rev. Lett. **97**, 045504 (2006).
[3] A.R. Oganov and C.W. Glass, J. Phys.: Condens. Matter **20**, 064210 (2008); A.R. Oganov *et al.*, Nature (London) **457**, 863 (2009).
[4] G. Hautier *et al.*, Chem. Mater. **22**, 3762 (2010).
[5] L. Lanier, G. Metauer, and M. Moukassi, Mikrochim. Acta **114/115**, 353 (1994); S. Watanabe, H. Ohtani, and T. Kunitake, Transactions ISIJ **23**, 120 (1983).
[6] I. Campos *et al.*, Mater. Sci. Eng. **A352**, 261 (2003).
[7] S. Sen, U. Sen, and C. Bindal, Vacuum **77**, 195 (2005).
[8] T. van Rompaey, K.C. Hari Kumar, and P. Wollants, J. Alloys Compd. **334**, 17 3 (2002).
[9] V.A. Barinov *et al.*, Phys. Stat. Sol. A **123**, 527 (1991); T. Kanaizuka, Phys. Stat. Sol. A **69**, 739 (1982).
[10] K. Balani, A. Agarwala, and N.B. Dahotre, J. Appl. Phys. **99**, 044904 (2006).
[11] K. Moorjani *et al.*, J. Appl. Phys **57**, 3445 (1985).
[12] L.G. Voroshnin *et al.*, Met. Sci. Heat Treat. [Metal. i Term. Obrabotka Metal.] **12**, 732 (1970).
[13] J.K. Burdett, E. Canadell, and G.J. Miller, J. Am. Chem. Soc. **108**, 6561 (1986).
[14] J.K. Burdett and E. Canadell, Inorg. Chem. **27**, 4437 (1988).
[15] P. Mohn and D.G. Pettifor, J. Phys. C: Solid State Phys. **21**, 2829 (1988).
[16] P. Mohn, J. Phys. C: Solid State Phys. **21**, 2841 (1988).
[17] W.Y. Ching *et al.*, Phys. Rev. B **42**, 4460 (1990).
[18] P.R. Ohodnicki, Jr. *et al.*, Phys. Rev. B **78**, 144414 (2008).
[19] G. Bergerhoff and I.D. Brown, in *Crystallographic Databases*, edited by F.H. Allen *et al.* (International Union of Crystallography, Chester,1987).
[20] J.J. Zuckerman and A.P. Hagen, (EDT), Inorganic Reactions And Methods (2007).
[21] J. Nagamatsu *el al.*, Nature (London) **410**, 63 (2001).
[22] H.-Y. Chung *et al.*, Science **316**, 436 (2007).
[23] I.I. Mazin *et al.*, Phys. Rev. Lett. **101**, 057003 (2008); M. Wierzbowska, Eur. Phys. J. B **48**, 207 (2005). S.K. Bose J. Phys.: Condens. Matter **21**, 025602 (2009).
[24] J.W. Simonson *et al.*, J. Supercond. Nov. Magn. **23**, 417 (2010) and references therein.
[25] Y. Kamihara *et al.*, J. Am. Chem. Soc. **130**, 3296 (2008); F.C. Hsu *et al.*, Proc. Natl. Acad. Sci. U.S.A. **105**, 14262 (2008); I.I. Mazin, Nature (London) **464**, 183 (2010).
[26] G. Kresse and J. Hafner, Phys. Rev. B **47**, 558 (1993); G. Kresse and J. Furthmüller, Phys. Rev. B **54**, 11169 (1996).
[27] See EPAPS Document No. 1.
[28] A.N. Kolmogorov, http://maise-guide.org.
[29] P. E. Blöchl, Phys. Rev. B **50**, 17953 (1994).
[30] J. D. Pack and H. J. Monkhorst, Phys. Rev. B **13**, 5188 (1976); **16**, 1748 (1977).
[31] J.P. Perdew, K. Burke, and M. Ernzerhof, Phys. Rev. Lett. **77**, 3865 (1996).
[32] L. Vočadlo *et al.*, Faraday Discuss. **106**, 205 (1997).
[33] M.J. van Setten *et al.*, J. Am. Chem. Soc. **129**, 2458 (2007).
[34] D. Alfè, Comp. Phys. Commun. **180**, 2622 (2009).
[35] P. Giannozzi *et al.*, http://www.quantum-espresso.org.
[36] We employ ultrasoft pseudopotentials [D. Vanderbilt, Phys. Rev. B **41**, R7892 (1990)] with a cutoff of 43 and 344 Ry for the wave functions and charge density, respectively. A $9 \times 9 \times 18$ k-point mesh with a Gaussian smearing of 0.02 Ry and a $3 \times 3 \times 6$ q-mesh are used for phonon dispersion calculations; a $18 \times 18 \times 36$ k-mesh is used to evaluate the e-ph coupling.
[37] D. Hohnke and E. Parthé, Acta Cryst. **20**, 572 (1966).
[38] G. Onida, L. Reining, and A. Rubio, Rev. Mod. Phys. **74**, 601 (2002).
[39] L. Topor and O.J. Kleppa, J. Chem. Thermodynamics **17**, 1003 (1985); A.F. Guillermet and G. Grimvall, J. Less-Common Met. **169**, 257 (1991).
[40] A.N. Kolmogorov and S. Curtarolo, Phys. Rev. B **74**, 224507 (2006) and references therein.
[41] M. Calandra and F. Mauri, Phys. Rev. Lett. **95**, 237002 (2005).
[42] A.Y. Liu, I.I. Mazin, and J. Kortus, Phys. Rev. Lett. **87**, 087005 (2001).
[43] P.B. Allen and R.C. Dynes, Phys. Rev. B **12**, 905 (1975).
[44] W.E. Pickett, Physica B **296**, 112 (2001).

Supplementary material to: New superconducting and semiconducting Fe-B compounds predicted with an *ab initio* evolutionary search

A.N. Kolmogorov,[1] S. Shah,[1] E.R. Margine,[1] A.F. Bialon,[2] T. Hammerschmidt,[2] and R. Drautz[2]
[1] *Department of Materials, University of Oxford, Parks Road, Oxford OX1 3PH, United Kingdom and*
[2] *Atomistic Modelling and Simulation, ICAMS, Ruhr-Universität Bochum, D-44801 Bochum, Germany*
(Dated: February 17, 2022)

Library of structure types We have considered over 40 commonly seen M-B and M-C structure types listed in the ICSD. The list below is ordered by composition and specifies the Pearson symbol and the prototype for each entry. 1:12: cF52-UB_{12}; 1:7: oI64-MgB_7; 3:20: oS46-Na_3B_{20}; 1:6: cP7-CaB_6; 3:14: tI160-Li_3B_{14}; 1:4: tP20-UB_4, oI10-CrB_4, mS10-MnB_4; 1:3: tP20-LiB_3, hP16-$Mo_{0.8}B_3$; 2:5: hR21-$Mo_2B_{4.65}$; 1:2: hP3-AlB_2, oP6-RuB_2, hR18-MoB_2, oP12-$PbCl_2$, hP6-ReB_2, hP6-MoS_2; 2:3: oS20-V_2B_3, hP10-Ru_2B_3; 3:4: oI14-Ta_3B_4; 5:6: oS22-V_5B_6; 1:1: oP8-FeB-b, oS8-$PtB_{0.67}$, tI16-MoB, oS8-TlI, oP8-TiSi, hP2-WC; 5:4: hP18-Rh_5B_4; 11:8: oP38-$Ru_{11}B_8$; 3:2: tP10-U_3Si_2, aP30-$Rh_9B_{5.5}$; 5:3: tI32-Cr_5B_3; 2:1: tI12-$CuAl_2$; 7:3: hP20-Th_7Fe_3, oP40-Mn_7C_3; 5:2: mS28-Mn_5C_2; 3:1: oP16-Fe_3C, oS16-Re_3B, tI32-Ni_3P; 23:6: cF116-$Cr_{23}C_6$; 4:1: tP10-Be_4B. Table I summarizes the lattice parameters and Wyckoff positions of the fully relaxed unit cells of the relevant ICSD and proposed phases.

Evolutionary algorithm (EA) search Module for *Ab Initio* Structure Evolution (MAISE) [1] takes advantage of the best EA strategies reported in the recent years [2–5] as well as our extensive tests to achieve fastest convergence for metal borides. The module creates input for VASP and gets back fully relaxed structures with the corresponding *ab initio* enthalpies. Starting sets of $N = 12$ structures are generated randomly. The population is then evolved through crossover (75%) and crossover plus mutation (25%); the mutation consists of shifts and swaps of the atoms as well as distortions of the unit cell. The best N members are selected from the pool of N old and N new members; the probability of survival is proportional to the fitness depending on the structure's enthalpy. Special care is taken to detect and eliminate similar structures in order to avoid stagnation. Fig. 1(a,b) demonstrates that diversity is maintained throughout the search (grey points) while the fittest member is always kept in the population (green points). Fig. 1(c) shows the lowest relative formation enthalpies obtained in three runs with different random seeds for each composition. Each run consisted of 50-100 generations, i.e., 600-1200 structural relaxations. Typically, all three runs converged to the same structure in no more than 60 generations.

Accuracy of the DFT approximations The 500 eV energy cutoff and dense k-meshes ensure numerical convergence of the formation energy differences to within

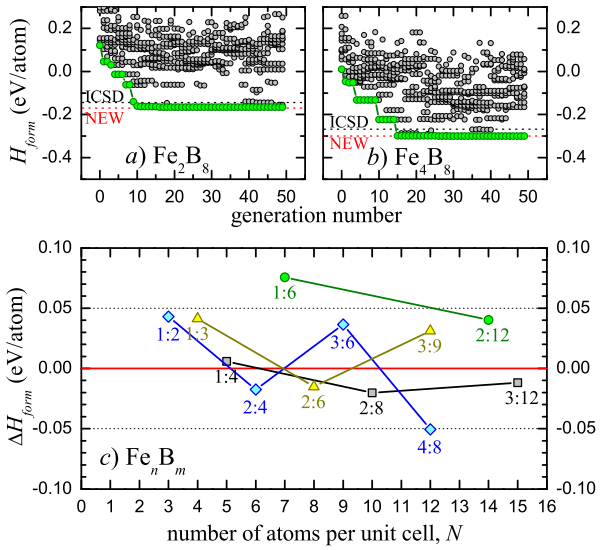

FIG. 1: *a,b*) Typical enthalpy distributions for competing structures during an EA-driven ground state search. In each generation 12 new members are fully relaxed with VASP; the best member shown in green is kept in the population. For 1:4 and 1:2 Fe-B compositions the evolutionary search finds new structure types, oP10 and oP12, significantly lower in enthalpy than the known ones from the ICSD. *c*) Relative formation enthalpies (referenced to the α-B↔oP8-FeB tie-line) of the most stable phases for each unit cell size found in the EA search; compounds with negative ΔH_{form} are thermodynamically stable w.r.t. the known α-B and oP8-FeB.

a few meV/atom but the systematic errors due to the approximated form of the xc functionals for the complex Fe-B system can be expected to be larger. Figure 1 shows dependence of the relative stabilities for predicted phases on the choice of commonly used DFT flavours: the Perdew-Zunger parameterization within the local density approximation (LDA) [6] and the Perdew-Burke-Ernzerhof (PBE) [7], Perdew-Wang (PW91) [8], and PBEsol [9] parameterizations within the generalized gradient approximation (GGA).

We observe that the relative stability of the boron-rich phases varies by over 30 meV/atom when simulated in GGA-PBE and LDA but in all the treatments the predicted FeB_2 and FeB_4 compounds are stable w.r.t. the α-B↔oP8-FeB tie-line. The systematic errors do not allow us to conclusively resolve the close in energy oP6-

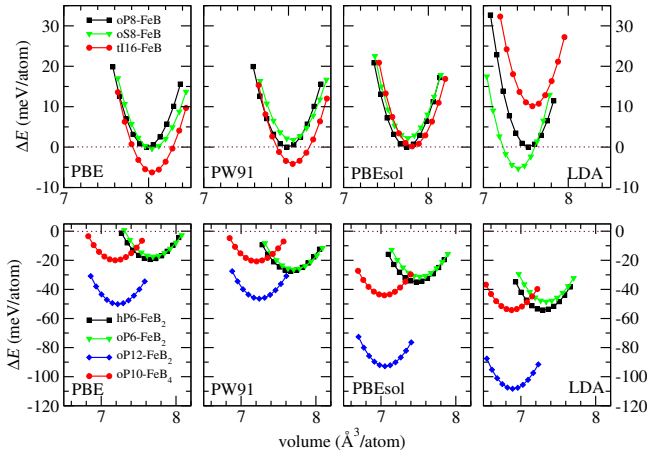

FIG. 2: E(V) curves for the competing crystal structures oP8, oS8, and tI16 at 1:1 composition relative to oP8 (upper panel) and the predicted structures at 1:2 and 1:4 composition (lower panel) relative to the α-B↔oP8-FeB tie-line.

FeB_2 and hP6-FeB_2 or tI16-FeB, oP8-FeB and oS8-FeB. However, oP10-FeB_4 is consistently below oI10-FeB_4 by ~ 25 meV/atom and hP3-FeB_2 is consistently above the α-B↔oP8-FeB tie-line by ~ 200 meV/atom. The thermodynamic corrections are found to be not sensitive to the choice of the DFT approximation and show similar T-dependences in the LDA and GGA-PBE.

Convergence of the e-ph calculations In order to check the convergence of λ we perform the calculations for two sets of grids: (i) the $2\times2\times4$ q- and $6\times6\times12$ k-meshes for the dynamical matrix and the $12\times12\times24$ $k-$mesh for the e-ph coupling (ii) the $3\times3\times6$ q- and $9\times9\times18$ k-meshes for the dynamical matrix and the $18\times18\times36$ k-mesh for the e-ph coupling. For the 0.02 Ry smearing in the k-point integration we find nearly identical values of $\lambda = 0.80$ (note that in these calculations the smearing leads to a lower value of $n(E_F) \approx 0.8$ states/(eV spin f.u.) due to a large gradient of the DOS near the Fermi level). We also find negligible changes (below 0.4 cm^{-1}) in Γ-point frequencies when the k-mesh is increased from $9\times9\times18$ to $12\times12\times24$ and $15\times15\times30$.

	Space group	a (Å)	b (Å)	c (Å)	β	Wyckoff positions B		Wyckoff positions Fe	
oP8-FeB	62	5.409	2.948	3.997		4c	(0.0344, 1/4 , 0.6186)	4c	(0.1779, 1/4 , 0.1203)
oS8-FeB	63	2.896	7.521	2.949		4c	(0 , 0.4306, 1/4)	4c	(0 , 0.1429, 1/4)
tI16-FeB	141	2.931	2.931	14.971		8e	(0 , 1/4 , 0.7151)	8e	(0 , 1/4 , 0.1791)
hP3-FeB_2	191	3.030		2.749		2c	(1/3 , 2/3 , 0)	1b	(0 , 0 , 1/2)
oP6-FeB_2	59	4.411	2.778	3.764		4f	(0.0467, 1/4 , 0.6428)	2a	(1/4 , 1/4 , 0.1504)
hP6-FeB_2	194	2.805		6.737		4f	(1/3 , 2/3 , 0.5567)	2c	(1/3 , 2/3 , 1/4)
oP12-FeB_2	62	4.816	4.807	3.740		8d	(0.1611, 0.0693, 0.3930)	4a	(0.0198, 1/4 , 0.8761)
mP8-FeB_3	11	3.813	2.819	5.527	100.974	2e	(0.1766, 1/4 , 0.0596)	2e	(0.9137, 1/4 , 0.6891)
						2e	(0.3759, 1/4 , 0.5476)		
						2e	(0.4872, 1/4 , 0.8831)		
oI10-FeB_4	71	4.518	5.287	3.052		8n	(0.2121, 0.3407, 0)	2a	(0 , 0 , 0)
oP10-FeB_4	58	4.521	5.284	3.006		4g	(0.1606, 0.1267, 0)	2c	(0 , 1/2 , 0)
						4g	(0.7508, 0.1871, 0)		
mS30-FeB_4	12	13.961	2.936	5.316	96.256	4i	(0.7515, 0 , 0.7495)	2b	(0 , 1/2 , 0)
						4i	(0.1124, 0 , 0.1584)	4i	(0.1610, 0 , 0.5467)
						4i	(0.9164, 0 , 0.1609)		
						4i	(0.7864, 0 , 0.0661)		
						4i	(0.4481, 0 , 0.3587)		
						4i	(0.5817, 0 , 0.3346)		

TABLE I: Space groups, lattice parameters, and Wyckoff-positions of fully relaxed Fe-B structures.

[1] A.N. Kolmogorov, http://maise-guide.org.

[2] D.M. Deaven and K.M. Ho, Phys. Rev. Lett. **75**, 288 (1995).

[3] A.R. Oganov and C.W. Glass, J. Chem. Phys. **124**, 244704 (2006).
[4] A.R. Oganov and C.W. Glass, J. Phys.: Condens. Matter **20**, 064210 (2008).
[5] N.L. Abraham and M.I.J. Probert, Phys. Rev. B **73**, 224104 (2006).
[6] D.M. Ceperley and B.J. Alder, Phys. Rev. Lett. **45**, 566 (1980); J.P. Perdew and A. Zunger, Phys. Rev. B **23**, 5048 (1981).
[7] J.P. Perdew, K. Burke, and M. Ernzerhof, Phys. Rev. Lett. **77**, 3865 (1996).
[8] J.P. Perdew, J.A. Chevary, S.H. Vosko, K.A. Jackson, M.R. Pederson, D.J. Singh, and C. Fiolhais, Phys. Rev. B **46**, 6671 (1992).
[9] J.P. Perdew, A. Ruzsinszky, G.I. Csonka, O.A. Vydrov, G.E. Scuseria, L.A. Constantin, X. Zhou, and K. Burke, Phys. Rev. Lett. **100**, 136406 (2008).